A finite-length-dipole model of the double layer in polar, polarizable materials

J. Ross Macdonald and S. W. Kenkel
Department of Physics and Astronomy, University of North Carolina, Chapel Hill, North Carolina 27514

(Received 6 May 1983; accepted 15 November 1983)

Because no relatively simple theory exists for the electrical double layer in polar, polarizable material such as an aqueous electrolyte, we develop here and solve in closed form, a semidiscrete lattice gas double layer theory applicable over a range of applied potential difference up to that leading to full dielectric saturation. It considers for the first time in the present context solvent molecules with *finite-length* permanent dipoles and induced ideal dipoles. The latter dipoles are treated in two distinct ways: semidiscretely or as leading to a continuum background dielectric constant ϵ_∞. We consider statistical averaging of the permanent dipoles in a given layer over all possible orientations and include competition for lattice-site occupancy between ions and solvent molecules self-consistently. Results for the diffuse region with multiple lattice layers and finite ionic concentration will be discussed in subsequent work. Here the full equations are first developed and then specialized for the case of a charge-free molecular monolayer at a metal electrode; they thus apply best to an adsorption situation or to the inner Helmholtz layer region of the full electrical double layer, but their predictions are compared with bulk dielectric constants as well. We present the dependences of various electrical quantities of interest on position across the monolayer and on applied field and permanent dipoles (p.d.), with the monolayer taken between two conducting plates. The semidiscrete treatment of the induced polarizability leads to a ferroelectric Mossotti catastrophe, but that for the finite-length permanent dipoles alone does not. The present work also demonstrates that the finite-length dipole model leads to negligible dielectric saturation, when applied to water molecules, e.g., up to fields larger than those expected to occur in the actual aqueous electrolyte double layer. This surprising result is a direct consequence of the behavior of the finite-length rather than the ideal permanent dipoles assumed in other treatments of the dielectric constant and dielectric saturation.

I. INTRODUCTION

The ionic diffuse double layer, which consists of a space charge region near a phase change or electrode, plays a very important role in the electrical behavior of solid and liquid electrochemical systems, colloids, and living cells. But there does not currently exist a theory of the ionic double layer at a completely blocking metal electrode in liquid electrolytes which is adequate in the charge/potential region where ions and solvent molecules begin to approach saturated conditions. We present here a semimicroscopic theory which attempts to meet this need.

There are two common approaches to the problem of treating the behavior of a large quantity of discrete particles: the continuum and statistical methods. In the first of these, the particles are taken as infinitely numerous points, smoothly filling a region of space of interest. The first double layer theory, that of Gouy and Chapman,[1,2] is of this type and becomes wholly inadequate when finite particle size plays a dominant role, e.g., at high concentration and even at low concentration near saturation. In the statistical method, on the other hand, discreteness is accepted but only average behavior is considered, again representing a particular idealization of reality. Many modern statistical treatments of the double layer in a liquid[3–9] have considered discrete charges but represented the liquid by a continuum with homogeneous field-independent bulk dielectric constant ϵ_B. A few recent ones have, more realistically, represented the solvent by taking the discrete molecules as hard spheres with permanent ideal or finite-length dipole moments.[10–14] These dipole theories have the great advantage of including such effects as dielectric saturation and hydration in a natural way. Especially in regions where large spatial gradients of potential exist, as in the space immediately next to a blocking electrode with an appreciable applied potential difference, ideal-dipole treatments will be inadequate since the use of a point–dipole model to represent a finite-size molecular dipole is equivalent to averaging over a region comparable to a solvent molecule in size. Further, all these valuable treatments are invariably very complicated and have not yielded adequate results for the approach to saturation. For these reasons one of the authors and his associates have considered some simpler but more approximate lattice–gas treatments of the diffuse double layer which allow saturation to be closely approached. The lattice gas approach, while quite appropriate for single crystal solids, is an approximation for liquids but one which has, nevertheless, been found quite useful in the theory of liquids.

Previous papers have dealt with various lattice–gas approaches to the calculation of accumulation-type space-charge equilibrium distributions near blocking electrodes in solids and liquids with charges of both signs mobile. Earlier work[15–18] employed continuum differential equations and the homogeneous field-independent bulk dielectric constant ϵ_B. In order to treat regions of high charge-carrier concentration near the electrode more exactly, the continuum ap-

 0021-9606/84/052168-15$02.10

proximation was partly eliminated by considering a model involving an infinite number of discrete two-dimensional lattice–gas charged layers parallel to the electrode.[19] Thus, differential equations were replaced with difference equations. This analysis was particularly appropriate for single crystals. Next, part of the bulk dielectric constant approximation was eliminated in order to try to achieve a more realistic treatment of the double layer in liquid electrolytes. A field-independent contribution to the bulk dielectric constant arising from induced polarizability alone ϵ_∞ was added to the effects of solvent–molecule permanent dipole moments. These permanent dipoles were taken as ideal but their polarization was spread out perpendicular to the electrode to account approximately for the finite size of actual solvent molecules. This approach[20–22] replaced each of the charged layers of the previous work by three charged layers, with the outer layers having equal and opposite charges and thus fully representing the effect of the region of constant polarization between them. Although this treatment appears to provide a useful advance over earlier ones, it does not treat the effects of the finite length of solvent–molecule permanent dipoles and induced polarizability accurately and discretely.

Therefore, in the present work we shall consider a somewhat more realistic semistatistical model in which the material is again divided into lattice–gas layers but ones with each lattice site capable of being occupied by a positive or negative ion of finite size or by a finite-size solvent molecule. We take such molecules as carrying a rotatable finite-length permanent dipole and as being polarizable as well. Each layer thus has a thickness determined by the lattice spacing. We solve the site competition problem for each layer by the statistical method, then average laterally over all particles in the plane of the layer. Although it was assumed in Ref. 22 that there might be present finite-thickness $\epsilon = \epsilon_\infty$ regions without permanent dipole polarization between each triple layer and its adjacent triple-layer neighbors, here we make the more realistic assumption for an averaged situation that each finite-thickness layer directly abuts its nearest neighbors. Finally, an infinite number of such layers parallel to a completely blocking electrode at $x = 0$ is considered and the layers are coupled together using one-dimensional electrostatic relations involving x-dependent average field, charge, and potential. In the present paper, the equations for this complete ion–molecule double layer problem will be fully developed but applied only to the electrical behavior of a single absorbed layer of polar, polarizable molecules. In a subsequent paper, the solution of the full double layer problem for the present model will be presented. In the next section the equations are developed and in the following one results for an adsorbed layer are presented and discussed.

It is worth pointing out some connections between the present lattice–gas treatment of a system containing ions and polar, polarizable discrete molecules and experimental and theoretical treatments of certain polar solids. An electrical analog of a spin glass is the dipole glass, where electric dipoles are arranged randomly.[23] Such a material is not likely to be very different in its equilibrium electric properties from our present liquid electrolyte situation at a given instant in time or in terms of time-averaged electrical properties. Further, single crystals may contain ions arranged regularly on a lattice with effective permanent dipole moments.[23] For these materials, a lattice–gas treatment is particularly appropriate, although there are generally only a few different dipole orientations possible in single crystals, while we consider all possible orientations in the present work.

II. THE FULL MODEL

We consider a system of N_V particles per unit volume, consisting of solvent molecules and uni–univalent solute ions of concentration c_0. Let $\delta \equiv c_0/N_V$. Then the molarity

$$M_0 \cong (6.022 \times 10^{20}) c_0,$$

where c_0 is measured in number per cm^{-3}. A number δN_v of the particles consists of anions, and there are an equal number of cations. The remaining $(1 - 2\delta) N_v$ particles are molecules with permanent dipole moment μ. Each dipole is represented by two point charges, of magnitude ηe, separated by a distance $d \equiv 2t$. Thus the dipole moment is $\mu = \eta e d$. In some instances we may choose to take polarizability of the particles into account by assigning each type of particle a polarizability α_i, which may be 0. Each particle is modeled as a hard sphere of diameter $a \equiv N_V^{-1/3}$. The hard sphere repulsive potential is accounted for by the lattice gas treatment.

We assume that the effects of the induced polarizabilities of the ions and solvent molecules can be approximately taken into account by a homogeneous background dielectric constant ϵ_∞, much smaller than the bulk dielectric constant of the solvent alone ϵ_B. At sufficiently high fields or frequencies we expect ϵ_{eff}, the effective dielectric constant of the overall system to approach ϵ_∞. In order to investigate the effect of the induced polarization of solvent molecules when no ions are present by a semidiscrete approach, however, we shall assume that $\alpha_s \equiv \alpha$, the polarizability of solvent molecules, is not necessarily zero even when $\epsilon_\infty > 1$. By this means, our approach will include the situations of physical interest $\epsilon_\infty \geqslant 1$, $\alpha \geqslant 0$.

In the present work, we consider a single lattice plane and its occupants. In future work, we shall employ the present single-layer solution to build up the solution for the equilibrium electric response of an infinite number of layers. Although we shall here consider only the no ion or zero molarity situation in detail, we present the basic equations of the full solute–solvent system in order to use these equations in future multiple-layer work based on the present finite-dipole model. When our general finite-length dipole equations are specialized for the single layer, zero molarity case with $\alpha = 0$ and $\epsilon_\infty > 1$, they become equivalent to those derived earlier by Oldham and co-workers.[24,25] Our full analysis and the monolayer investigation of the present paper were carried out independently of this pioneering work before its existence was known to us. We develop herein the more general equations for a multiple-layer nonzero-molarity situation with semidiscrete treatment of the induced polarizability ($\alpha > 0$). Thus, our approach includes the statistical competition for lattice site occupancy between positive and negative ions and polar, polarizable molecules. Even in the monolayer for the $\alpha = 0$ and $\epsilon_\infty > 1$ case, where our work overlaps with that of Oldham *et al.*, we have elected to con-

sider $\epsilon_{\rm eff}$, dielectric saturation, specific position dependence of electrical variables within an average layer, and high-field response, while Oldham *et al.* were primarily concerned with the differential capacitance of the monolayer. Further, we make specific comparisons between results arising from the two different ways of taking the molecular polarizability into account and find large differences between them.

For the general case, we begin by erecting a three-dimensional cubic lattice with lattice spacing a. Each lattice point may be occupied by only one particle, either a positive or negative ion or a polarizable molecule. The ions are represented by point charges at the lattice sites. The polar, polarizable molecules are represented by finite-length permanent dipoles, centered on the lattice sites, and infinitesimal induced dipoles at the sites. In order to simplify the mathematics, we consider only the variation in the direction perpendicular to the electrode, the x direction. All quantities thus represent an average over the plane at a given x position. The resulting effective field and "smeared" charge treatment are not identical to the introduction of mean field approximations, but our self-consistent averaged approach does include many of the same feedback effects. Although no explicit detailed account is taken of cooperative effects, such as short-range dipole ordering, there is a field at a position where an ion or dipole could be which depends directly on the average charge density in the given layer. Even though further introduction of explicit mean field effects is possible,[16,18] we have omitted them from the present treatment in the interest of simplicity. We begin by considering an arbitrary lattice plane, indicated by the superscript i. In general, unsuperscripted quantities are used to refer to a single lattice plane, and superscripts are used to show the relations between one plane and the next.

As already mentioned, in the present work we take $d = a$, equivalent to the assumption that the finite-dipole point charges lie at the ends of a molecular sphere diameter. The case $d < a$ has been analyzed in earlier more approximate work on the present problem[22] where many layers containing ions and dipoles are assumed present. When $d < a$, a layer of thickness $(a - d)$ and dielectric constant ϵ_∞ is interposed between each finite-dipole molecular layer. It has low capacitance, since it contains only induced infinitesimal dipoles, and the capacitance of such layers is in series with that from all the finite-dipole layers. In the earlier work it was found that $(a - d)/a$ had to be small or the theory could not yield experimental bulk capacitance results. We expect the same effect to occur here and have eliminated it by taking $d = a$. The problem is introduced by the present essentially one-dimensional lattice–gas treatment. In an actual material, thermal agitation tends to average out most $d < a$ effects and no $(d - a)$-thick layers parallel to the electrode would occur. By taking $d = a$ but, in addition, introducing the disposable relative finite-dipole-moment strength factor λ, we gain sufficient flexibility to make the present idealized model useful.

Let $y \equiv x/t$, our basic normalized distance variable. Since we take $d \equiv a$, $-1 \leqslant y \leqslant 1$ defines the diameter of a solvent molecule. Let $\psi(x)$ be the average local potential in this region, defined as the potential whose derivative gives the average force on a negative test charge, the local electric field. Thus

$$E(x) \equiv -d\psi/dx.$$

Let us now use the thermal potential $V_N \equiv kT/e$ to normalize ψ, so

$$\phi \equiv \psi/V_N. \tag{1}$$

Take the normalizing field E_N as V_N/t. Then,

$$E^*(y) \equiv E(x)/E_N = -(d\phi/dy). \tag{2}$$

It is useful at this point to define several other normalizing constants and conversion factors. A natural unit of length is the lattice Debye length,

$$L_{DN} \equiv [\epsilon_\infty kT/8\pi e^2 N_V)^{1/2}. \tag{3}$$

It is also found useful to define a dimensionless constant which scales as the dipole length,

$$T_N \equiv t/L_{DN}. \tag{4}$$

Finally, we may define a normalizing planar charge density as

$$\sigma_N \equiv \epsilon_\infty kT/4\pi et \equiv C_N V_N, \tag{5}$$

where C_N is a normalizing capacitance per unit area. We shall normalize volume charge densities with (σ_N/t).

Now the (normalized) fields and potentials within the ith layer are given by $E^*(y)$ and $\phi(y)$. The values at the left, center, and right of a layer are

$$E^*(-1) \equiv E^{*i}_{-1}, \quad \phi(-1) \equiv \phi^i_{-1},$$
$$E^*(0) \equiv E^{*i}_0, \quad \phi(0) \equiv \phi^i_0, \tag{6}$$

and

$$E^*(1) \equiv E^{*i}_1, \quad \phi(1) \equiv \phi^i_1.$$

The boundary conditions which link one layer to the next are simply continuity:

$$E^{*i}_{-1} = E^{*i-1}_1, \quad \phi^i_{-1} = \phi^{i-1}_1, \tag{7}$$

with

$$i = 2,3,\ldots .$$

At the first layer, next to the electrode,

$$E^{*1}_{-1} = Q_m, \quad \phi^1_{-1} = \phi_a. \tag{8}$$

Here Q_m is the (normalized) charge per unit area on the electrode, and ϕ_a is the applied potential difference, with ϕ at $x = \infty$ taken zero. Note that Q_m is equal and opposite to the sum of the net charges of all the layers between $x = 0$ and ∞ for the present completely blocking electrode situation.

Within each layer the fields and potentials are determined by the effective overall charge density, which is related to the particle occupancy and average dipole orientation. From now on, we shall consider only the monolayer, $i = 1$, situation. Since we are interested in low frequency or *dc* response, we may use equilibrium statistical mechanics to find the number of particles of each type present at each lattice layer. These numbers depend on the electrostatic energy of the particles u_j, given in normalized form by

$$U_j \equiv u_j/kT, \tag{9a}$$

with

$$U_C = \pm\phi_0, \tag{9b}$$

$$U_D = \eta[\phi(y) - \phi(-y)], \tag{9c}$$

and

$$U_\alpha = -(\alpha\beta/2kT)E_0^2. \tag{9d}$$

In Eq. (9d), the normalized E_0 is not the full $E^*(0)$ of Eq. (6) but, for self-consistency, it is that field minus the induced ideal dipole self-field, which involves a delta function at $y = 0$. The subscript j denotes the charges (C), the permanent dipoles (D), or the induced dipoles (α). Here β is a constant which is used to approximately account for the depolarizing field caused by surrounding induced dipoles in the true three-dimensional situation. This field leads to a feedback which can effectively enhance or reduce α. The statistical mechanics is contained in the partition function

$$Z_T \equiv \frac{1}{N_V}\sum_j n_j \exp(-U_j), \tag{10}$$

where n_j is the bulk number density of particle type j. We may separate the partition function into the contributions from the charges,

$$Z_C = \sum_{z=\pm 1} \delta \exp(-z\phi_0) = 2\delta\cosh(\phi_0), \tag{11}$$

and the part associated with the dipoles,

$$\begin{aligned} Z_D &= (1-2\delta)\int_{-1}^{1} \exp[-\{U_D(y) + U_\alpha\}]dy \\ &= (1-2\delta)\Pi_\alpha \int_0^1 \cosh[U_D(y)]dy, \end{aligned} \tag{12}$$

where

$$\Pi_\alpha \equiv \exp(-U_\alpha). \tag{13}$$

The integral in Eq. (12) is over all allowed orientations of the dipoles. The Π_α term is the contribution of the induced dipoles, which does not depend on permanent dipole orientation. There is no similar term in Eq. (11), as we are neglecting the polarizability of the ions. If we define θ as the angle between the dipole orientation and the local field direction $y = \cos(\theta)$. For simplicity, we assume a continuum model in which any orientation is possible. The frequency with which a given orientation occurs is determined by the electrostatic energy of the dipole in that configuration u_D. Note that in the case of a uniform electric field E this energy is the standard dipole energy $u_D = \mu E\cos(\theta)$. In the present case, however, the dipole energy and the partition function are nonlocal functions of the field.

The partition function allows us to calculate the number of charges and the number of dipoles in every orientation, given the potential at every point y. This potential is influenced by the charges and dipoles and thus must be calculated self-consistently. One way of calculating the potential is to use a smeared charge approximation in which we replace the discrete charges by sheets of charge of the appropriate charge density. This is entirely consistent with the one-dimensional nature of the problem.

The appropriate volume charge density follows from the partition function and a generalization of the thermodynamic result,

$$\rho = d\{kT\ln(Z)\}/d\psi.$$

Here ψ is the conjugate variable to the charge density ρ and the derivative is interpreted in the sense of the functional derivative. Specifically, the ions involve a delta function in surface charge density at the layer lattice points ($x = 0$), and their bulk charge density may be written

$$\begin{aligned} \rho_I &= (\delta a e N_V/Z_T)(e^{\phi_0} - e^{\phi_0})\delta(x) \\ &= (2\delta a e N_V/Z_T)\sinh(\phi_0)\delta(x). \end{aligned} \tag{14}$$

Each finite-length dipole involves a charge at y and an equal and opposite charge at $-y$. Thus the charge density due to the dipoles at position y is a function of the number of dipoles in the orientations $\cos(\theta) = y$ and $\cos(\theta) = -y$,

$$\begin{aligned} \rho_D(y) &= [(1-2\delta)\eta e N_V(\Pi_\alpha/Z_T)][e^{-U_D(y)} - e^{-U_D(-y)}] \\ &= -2\eta e N_V(1-2\delta)(\Pi_\alpha/Z_T)\sinh[U_D(y)]. \end{aligned} \tag{15}$$

The induced dipoles may be taken as contributing a charge doublet at the origin

$$\rho_\alpha(x) = -(1-2\delta)(N_V a\alpha\beta E_0)(\Pi_\alpha/Z_T)\delta'(x). \tag{16}$$

The electrostatics now consist of the one-dimensional Poisson equation,

$$\frac{dE}{dx} = 4\pi\rho(x)/\epsilon_\infty,$$

or in normalized form,

$$\frac{dE^*}{dy} = \rho(y)/\sigma_N, \tag{17}$$

and the definition of the electric field $E^* \equiv -d\phi/dy$, where

$$\rho(y) = \rho_D(y) + \rho_\alpha(y) + \rho_I(y). \tag{18}$$

The combination of Eqs. (9)–(11) and (14)–(18) forms a complicated set of nonlinear integro-differential equations. In addition, Z_T is a nonlocal function of potential, and must be calculated self-consistently. These equations can be solved analytically in terms of elliptic functions (see the Appendix), or, in the low-field limit, in terms of elementary functions.

The equations become somewhat simpler by introducing variables which take advantage of the symmetry of the problem. From Eq. (17), the field can be written as

$$\begin{aligned} E^*(y) &= E^*_{-1} + \frac{1}{\sigma_N}\int_{-1}^{y} \rho(y')dy' \\ &= E^*_{-1} + \frac{1}{\sigma_N}\int_{-1}^{0} \rho_D(y)dy + Q_I U_0(y) + \frac{1}{\sigma_N} \\ &\quad \times \int_0^y \rho_D(y')dy' + Q_\alpha\delta(y), \end{aligned} \tag{19}$$

or

$$E^*(y) \equiv E^*_{-1} - Q_{D1} + Q_I U_0(y) + Q_D(y) + Q_\alpha\delta(y), \tag{20}$$

where

$$Q_I = -2\delta T_N^2\sinh(\phi_0)/Z_T, \tag{21a}$$

$$Q_D(y) \equiv \sigma_N^{-1}\int_0^y \rho_D(y')dy', \tag{21b}$$

$$Q_{D1} \equiv Q_D(1), \tag{21c}$$

and

$$Q_\alpha \equiv -2BE^*_0. \tag{22}$$

Here $U_0(y)$ is a unit step function, and the constant

$$B \equiv 4\pi N_V(1-2\delta)\alpha\beta(\Pi_\alpha/Z_T)/\epsilon_\infty$$

scales that part of the voltage drop in a layer due specifically to the induced polarizability. It is useful to define the related constant $B_0 \equiv B(Z_T/\Pi_\alpha)$ the low-field limit of B. For convenience, in the rest of the paper we shall take $E^*(y)$ to mean $[E^*(y) - Q_\alpha \delta(y)]$, where the $E^*(y)$ within the brackets is that of Eq. (20). Then $E_0^* \equiv E^*(0)$ is the normalized field at the layer center except for induced dipole effects. Thus, we always take $E^*(0)$ in the figures and the rest of the text to mean just E_0^*. Now the potential can be expressed in terms of the "finite-length dipole potential," ϕ_D as

$$\phi(y) \equiv -\int_{-1}^{y} E^*(y')dy', \tag{23}$$

which leads to

$$\phi(y) = \phi_{-1} - (y+1)(E^*_{-1} - Q_{D1}) - (yQ_I + Q_\alpha)U_0(y) + \phi_D(y) + \phi_{D1}, \tag{24}$$

where

$$\phi_D(y) \equiv -\int_0^y Q_D(y')dy', \quad \phi_{D1} \equiv \phi_D(1). \tag{25}$$

Now all the variables can be found if the dipole variables ρ_D, Q_D, ϕ_D, and Z are known. The final set of equations becomes

$$Q_D(y) = \sigma_N^{-1} \int_0^y \rho_D(y')dy', \tag{26}$$

$$\phi_D(y) = -\int_0^y Q_D(y')dy', \tag{27}$$

$$Z = \int_0^1 \cosh[U_D(y)]dy, \tag{28}$$

and

$$Z_T = 2\delta \cosh(\phi_0) + (1 - 2\delta)\Pi_\alpha Z, \tag{29}$$

together with Eqs. (9c) and (15). It is important to emphasize that because of the coupling between the equations they must all be solved self-consistently.

III. RESULTS FOR A MOLECULAR MONOLAYER

The complete analytical results for a single lattice gas layer containing finite-size ions and polar, polarizable molecules have been presented in Sec. II and the Appendix. In the present situation where it is assumed that no ions are present ($\delta = 0$), the analytical solution of the problem is considerably simplified but remains implicit for any normalized applied p.d., ϕ_a, comparable to or greater than one. Except in the limit of small ϕ_a, one must solve the implicit Eq. (A5) for the partition function Z before Eqs. (A1) and (A2) may be used to obtain final results. The solution for self-consistent Z is straightforward, although it is found that Z becomes very large as $|\phi_a|$ increases, even within its experimental range of $0 < |\phi_a| \lesssim 35$. In this section, we present computer-calculated self-consistent results for the various monolayer electrical quantities of interest.

Although the equations developed earlier and in the Appendix apply to a single layer, they are in a form appropriate for the complete double layer problem, where each layer is coupled to those next to it. We require a field to orient the permanent dipoles of the monolayer and to induce ideal dipoles at its center. It is therefore convenient to consider the monolayer as being between plane-parallel capacitor plates with a charge Q_m on the left and a charge $-Q_m$ on the right. The left plate may be taken as a metal electrode, and in terms of normalized quantities we may set $E^*(-1) \equiv Q_m$. Although the orienting field or charge may be considered in some cases to be a "natural" field arising from chemisorption and work function effects,[26] we shall here consider it only as being associated with the situation present in the inner, charge-free region of the double layer. For present purposes it is then necessary to assume that all the potential drop occurs across the inner layer, and the diffuse ionic double layer region abutting it at the right acts as a perfect conductor and imager. This assumption will allow us to consider inner layer molecular effects apart from anything else. In the analysis of the full double layer, to be considered in a subsequent paper, this assumption is modified since although most of the applied p.d. occurs across the inner charge-free region, there will always be a small part of the total p.d. across the diffuse layer. It should be noted that the present monolayer will not act like a region of constant polarization as in a macroscopic capacitor. Since its total polarization will be a function of position, the actual internal local average field $E^*(y)$ will not be independent of position, although from symmetry it is clear that it must be an even function of y.

In the rest of the paper, we shall be concerned with two limiting cases for the effect of induced ideal–dipole polarization. In the semi-discrete situation of case (a) $B_0 > 0$ and $\epsilon_\infty = 1$ while for the semicontinuum approach of case (b) $B_0 = 0$ and $\epsilon_\infty = 6$. The appropriateness of this value of ϵ_∞ has been discussed elsewhere.[26] Let us begin by considering some case (a) results. Figure 1 shows the spatial dependence of the partial normalized charge ρ_D^* field, and potential from the left side of the monolayer, where we take $\phi(y) = \phi(-1)$, to the right side, where $\phi(y) = \phi(1)$. Here

$$\rho_D^*(y) \equiv \rho_D(y)/(\sigma_N/t)$$

is just the normalized effective dipole charge density arising from statistical averaging over all permanent dipole orientations. It does not contain the delta-doublet term arising from induced polarization [cf. Eq. (16)] or the $\delta(y)$ term which would be present if the ionic concentration were nonzero. All the results of Fig. 1 are for the relatively small value of E_0^* of unity. Curves are shown for three representative values of the polarizability constant B_0. All plotted curves are zero for $|y| \geqslant 1$ for a single monolayer.

Much of our results will be illustrated in terms of an aqueous electrolyte and will involve parameters appropriate for liquid water. For water at 20 °C,

$$N_V \cong 3.337 \times 10^{22}\ \text{cm}^{-3},$$

$$\alpha \cong 1.444 \times 10^{-24}\ \text{cm}^3,$$

and we take $\mu_v = 1.85$ D, the approximate vapor-phase value of the water permanent dipole moment. Then for case (a) with $\beta = 1$, $B_0 \cong 0.6$. We shall discuss more realistic choices for B_0 and β later. For the choice $d = 3.1$ Å, the pertinent normalization quantities are $V_N \cong 0.025\,26$ V, $E_N \cong 1.63 \times 10^6$ V/cm, $C_N \cong 5.712\ \epsilon_\infty\ \mu\text{F/cm}^2$, and σ_N

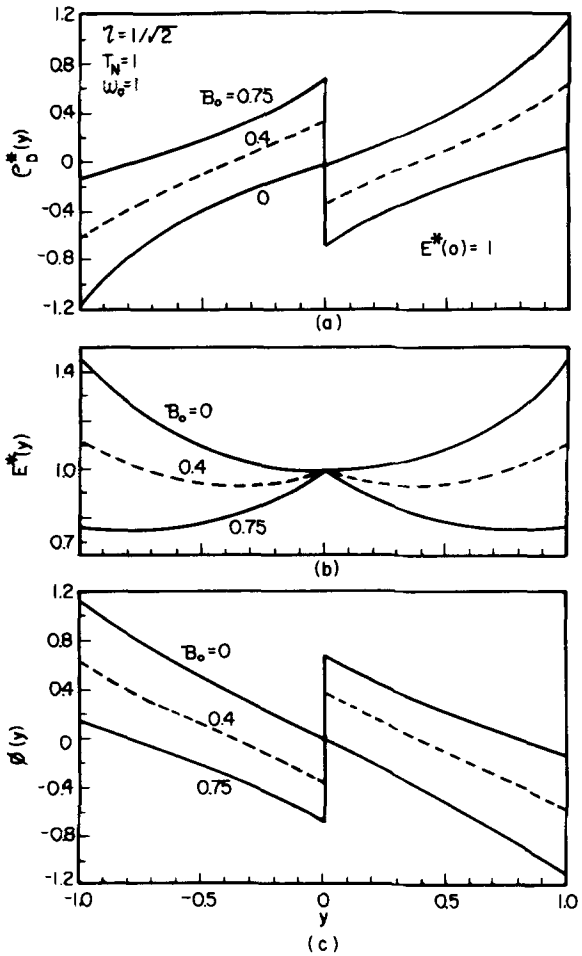

FIG. 1. Dependence of normalized dipole charge, field, and potential on position across the monolayer for $\omega_0 = 1$ and $E^*(0) = 1$.

$= 0.1443\,\epsilon_\infty\ \mu\text{C/cm}^2$.

Figure 1(a) shows that the effective permanent dipole charge density does not vary entirely linearly with position, even for the small value $E^*(0) = 1$. When $B_0 \neq 0$, the presence of the induced ideal dipole at $y = 0$ leads to the step function shown at this position. The values of η and T_N used in calculating the Fig. 1 results were selected for illustrative purposes and for convenience in such a way that

$$\omega_0 \equiv \sqrt{2}\eta T_N = 1.$$

Note that the permanent dipole moment

$$\mu \equiv \eta e(2t) \cong 9.6\eta T_N L_{DN}\ \text{D}$$

if L_{DN} is expressed in angstroms. For case (a), $L_{DN} \cong 0.0457$ Å and $\mu \cong 0.31$ D for the present choices of η and T_N. More realistic values of μ for water will be discussed later.

Figure 1(b) illustrates how $E^*(y)$ varies with y and B_0 for the specific choice $E^*(0) = 1$. Here the $\delta(y)$ term arising from the induced ideal dipole at $y = 0$ is not shown or included in $E^*(y)$. Clearly, the character of the $E^*(y)$ dependence changes significantly as B_0 increases. Finally, the curves of Fig. 1(c) show $\phi(y)$ dependence with the choice $\phi(0) = 0$. Note that

$$\phi_a \equiv \Delta\phi \equiv \phi(-1) - \phi(1).$$

Although these curves are nearly the negatives of the corresponding ones of Fig. 1(a), this is not a general result but merely an artifact of the various η, T_N, $\phi(0)$, and $E^*(0)$ values selected. For the $B_0 = 0$ case, $\phi_a \cong 2.25$, but ϕ_a is progressively reduced as B_0 increases because of the shielding effect of the center ideal dipole until $\phi_a \cong 0.3$ for $B_0 = 0.75$.

Figure 2 shows results for $(\epsilon_{\text{eff}})_0$, the $\phi_a \to 0$ limit of ϵ_{eff}, vs B_0 for various values of the dimensionless $\phi_a \to 0$ dipole moment variable $\omega_0 \equiv \sqrt{2}\eta T_N$. These results were calculated using Eq. (A54). Note that as $\omega_0 \to 0$,

$$(\epsilon_{\text{eff}})_0 \to (1 - B_0)^{-1}.$$

Further, for any ω_0, Eq. (A54) and Fig. 2 show that $(\epsilon_{\text{eff}})_0$, the ordinary small-signal effective dielectric constant of the monolayer, exhibits a pole when

$$B_0[\omega_0 \coth(\omega_0)] = 1.$$

Thus, the model leads to a ferroelectric transition at this point. This is the present analog of the Mossotti catastrophe described by Fowler[27] and von Hippel.[28] But there is an interesting difference here. As discussed by Fowler,[27] the ordinary Debye theory of gaseous electric susceptibility, involving *permanent* ideal dipoles, leads to the Mossotti catastrophe, but here the transition arises from the *induced* ideal dipoles and disappears for $B_0 \to 0$. We conclude that the reason there is no Mossotti catastrophe for the permanent dipoles [e.g., in case (b) with $B_0 = 0$] is because they are taken of finite length in the present nonlocal theory. As Onsager[29] and Kirkwood[30] have shown, for condensed systems inclusion of reaction field effects and association between dipole orientations eliminates the Mossotti catastrophe in treatments of polar materials involving point permanent dipoles.

In a real liquid, as opposed to a lattice–gas model, polarizable molecules move around continuously, thus spreading out over the space the electrical effect of each induced nearly ideal dipole. A measurement of $(\epsilon_{\text{eff}})_0$, even for a monolayer, yields the time and space averaged effect of many individual

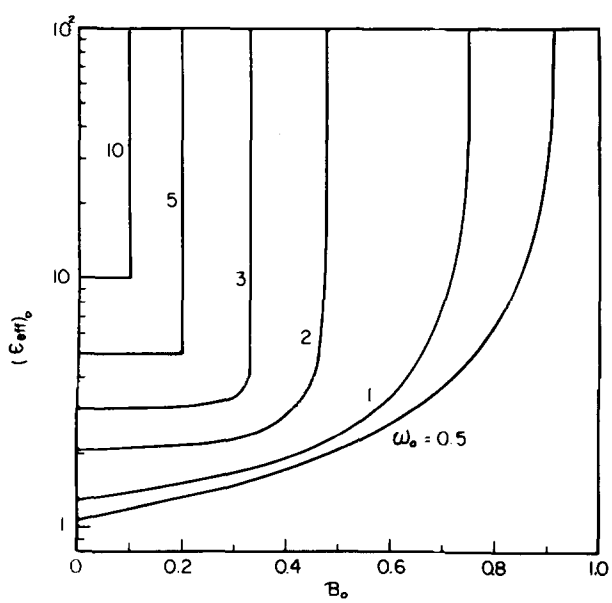

FIG. 2. Dependence of the low-field effective dielectric constant $(\epsilon_{\text{eff}})_0$ on the normalized polarization parameter B_0 for several values of the normalized dipole moment parameter ω_0.

ideal dipoles, and, of course, does not show ferroelectric behavior for most materials, even in the bulk. No such behavior appears either in a dipole glass, where the dipole arrangement is random.[23] But some single crystals involving permanent dipoles arranged regularly on a lattice do show a permanent polarization in the low temperature region.[23] Thus, we may conclude that it is in part the failure of our equilibrium lattice gas model to allow time and space smearing/averaging of ideal dipole positions which is associated with the present possibility of $(\epsilon_{\rm eff})_0 \to \infty$ behavior in a range of B_0 likely to be realizable in actual materials. Further, Fig. 2 shows that the larger the permanent dipole moment, the smaller B_0 and the polarizability necessary for this catastrophe to occur.

Although our present induced and permanent dipole treatment takes account of dipole surroundings and negative-feedback reaction-field effects only through the inclusion of the so far *ad hoc* factor β in B_0 for induced dipoles, and through the possibility of $\mu > \mu_V$ for permanent dipoles, we can improve the induced dipole approach in an empirical fashion by first considering how β depends on α and N_V in ordinary semicontinuum lattice treatments of condensed phases with some effects of dipole surroundings included.[31-33] For two-dimensional layers one finds[31] that $\epsilon_\infty = 1 + A\alpha N_V$, where $A \cong 9$ is the Topping enhancement factor arising from surrounding similarly oriented induced dipoles. This result is obtained if a depolarization factor β is introduced and taken as $(1 + A\alpha N_V)^{-1}$. Slightly generalizing to the present situation and replacing A by 4π, we take the negative feedback factor as

$$\beta = [1 + A_0 m_0]^{-1}, \tag{30}$$

where

$$A_0 \equiv 4\pi N_V \alpha/\epsilon_\infty, \tag{31}$$

and

$$m_0 \equiv \omega_0 \coth(\omega_0). \tag{32}$$

Then

$$B_0 = A_0/(1 + A_0 m_0), \tag{33}$$

a quantity always less than unity. When this expression is substituted in Eq. (A54), one finds

$$(\epsilon_{\rm eff})_0/\epsilon_\infty = m_0[1 + A_0\{m_0 - m_0^{-1}\omega_0^2\}], \tag{34}$$

a result which predicts no Mossotti catastrophe. It also leads to the expected result,

$$(\epsilon_{\rm eff})_0 = \epsilon_\infty + 4\pi N_V \alpha,$$

in the $\omega_0 \to 0$ limit. We have included ϵ_∞ in these equations for completeness, even though in the present case (a) situation we take $\epsilon_\infty = 1$. Notice that for $\omega_0 \gtrsim 3$ or so, $m_0 \cong \omega_0$ and Eq. (34) reduces to just

$$(\epsilon_{\rm eff})_0/\epsilon_\infty \cong m_0 \cong \omega_0,$$

totally independent of B_0. Even our original Eq. (A54) is likewise independent of B_0 for $\omega_0 \gtrsim 3$ except in the immediate region of the ferroelectric transition. Further, since in the present $\delta = 0$ situation $B \equiv B_0/Z$ and Z becomes much larger than unity as $|\phi_a|$ increases, it is clear that induced polarization effects associated with B must entirely disappear for appreciable $|\phi_a|$. For $\omega_0 \gtrsim 3$, the usual situation of interest for water, we see that there are no case (a) α effects as $|\phi_a| \to 0$ or as $|\phi_a| \to \infty$. As we shall show, there are, in fact, none of consequence in the intermediate $|\phi_a|$ range either for $\omega_0 \gtrsim 3$.

Thus, although the case (a) inclusion of the effects of induced polarization of discrete molecules in our theory has been instructive, it is clear that with a reasonable value of B_0, which takes into account negative feedback effects, there are little or no case (a) α effects of interest. Therefore, in most of the remaining part of the paper, we shall make the alternative case (b) choice, replacing $\epsilon_\infty = 1$, $B_0 > 0$, with $\epsilon_\infty > 1$, and $B_0 = 0$. We thereby replace discrete induced ideal dipoles by smeared-out material with a field independent dielectric constant ϵ_∞, more in keeping with actual space and time averaging effects present in a real material. For the actual value of ϵ_∞ used in the subsequent calculations, we choose 6, a reasonable value for water.[26] In the remainder of this work we shall be concerned with the dependence of various electrical quantities on the applied field or potential difference, in order to show saturation effects, and we will additionally examine the spatial dependence of the effective local dipole charge and potential for small and large applied p.d.'s.

Figure 3 presents some field-dependence results for the normalized effective dielectric constant quantity

$$h \equiv (\epsilon_{\rm eff} - \epsilon_\infty)/((\epsilon_{\rm eff})_0 - \epsilon_\infty)$$

previously used in the present context.[26] With the present normalization we do not need to distinguish between cases (a) and (b) when h is plotted, but the normalization tends to obscure actual unnormalized differences between the predictions of the two cases; thus some unnormalized results for $\epsilon_{\rm eff}$ will be presented later. We have elected to show $B > 0$ results here only for the small value $\omega_0 = 1$ because, as already mentioned, case (a) results with $B_0 > 0$ are virtually indistinguishable from those with $B_0 = 0$ unless B_0 is nearly equal to the ferroelectric transition value M_0^{-1}. For appreciable ω_0 values, such as four or more, differences only occur when B_0 has a value so close to that yielding the $(\epsilon_{\rm eff})_0$ pole that $(\epsilon_{\rm eff})_0$ is greatly enhanced (see Fig. 2). It is clear, how-

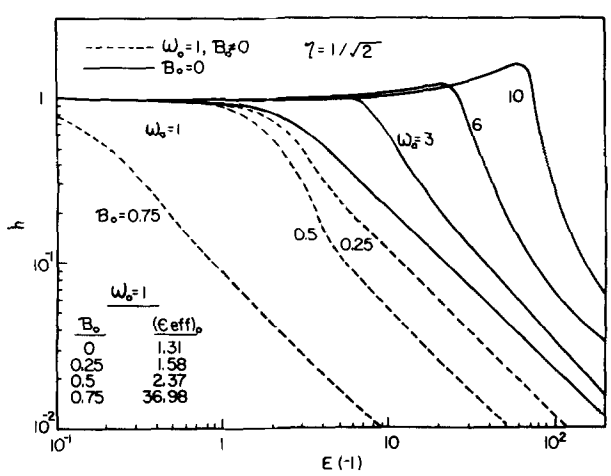

FIG. 3. Dependence of the normalized dielectric constant parameter h on normalized applied field $E^*(-1)$ for various ω_0 and B_0 choices [cases (a) and (b)].

ever, from Fig. 3 that for small ω_0 even B_0 values not close to the transition value can appreciably affect dielectric saturation curves. The $B_0 = 0$ curves show that as ω_0 increases, ϵ_{eff} actually increases with field before decreasing rapidly toward ϵ_∞. No such effect seems to occur for bulk water, but the present predictions of an initial increase may possibly be appropriate for a real monolayer.

In Fig. 4, we compare some $B_0 = 0$ results with ordinary Langevin saturation behavior.[21,22,26] This behavior, which was also found for the previous three-layer approximate finite dipole model, leads to

$$h = 3X_L^{-1}[\coth(X_L) - X_L^{-1}], \tag{35}$$

where

$$X_L \equiv \mu E/kT \equiv (\mu/et)E^*.$$

We choose the E^* acting on the point dipoles of the ordinary Langevin saturation model as E_0^*, with E_0^* always less than $E^*(-1)$. For our present water parameter choices, $X_L \cong 0.134\mu E_0^*$ when μ is expressed in Debyes.

We have chosen three different μ values for our curves here. The choice $\mu = 1.85$ D is that for vapor-phase water molecules. Second, we pick

$$(\epsilon_{\text{eff}})_0 = \epsilon_B \cong \epsilon_\infty \omega_0$$

and determine ω_0 and μ for the choice $\epsilon_B = 80.1$, the bulk value for water at 20 °C. This yields $\mu = 10.17$ D, close to the 9.5 D value used in the three-layer model for the correlation-augmented value of μ in liquid water. Finally, the $\mu = 17$ D value is that following[21,22] from the experimental water dielectric saturation measurements of Kolodziej and Jones.[34] We shall assume that $d = 2t = 3.1$ Å is the same for all these μ values, making $E_0^* \propto E_0$ for any μ. Then the three η values corresponding to these μ's are 0.124, 0.682, and 1.14, respectively. Note that η should not exceed unity for univalent dipole charges. The use of the large 17 D figure for Langevin-type dielectric saturation in water is likely to be a poor approximation, probably associated in part with the replacement of the actual water molecule tripole by a dipole. Nevertheless, the use of an effective dipole moment for liquid water greater than $\mu_V = 1.85$ D is a common way to account for some of the effects of reaction field and correlation on each permanent dipole.[29,30]

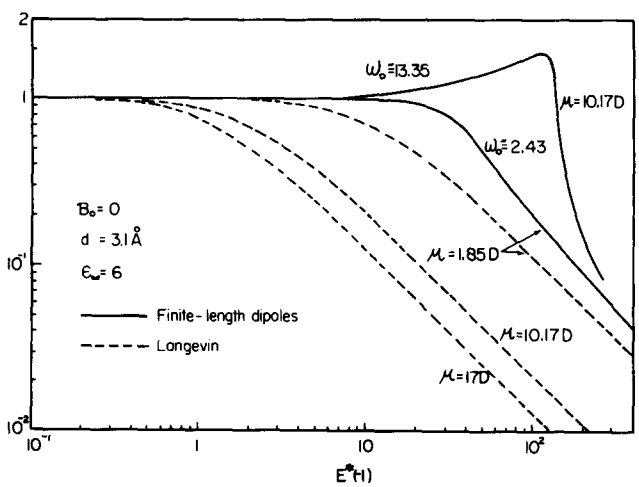

FIG. 4. Dependence of h on $E^*(-1)$ for case (b) with several μ and ω_0 values appropriate for water comparing finite-length dipole and Langevin dielectric saturation response.

The curves of Fig. 4 show that a Langevin dipole model leads to much more saturation at a given field than does the present finite-length dipole one. Further, the $\mu = 10.17$ D finite-length curve again shows a peak in h or ϵ_{eff} before a rapid decline. Clearly, increasing μ for a Langevin model causes a given degree of saturation to be achieved at a lower field the larger μ, but the opposite effect appears for the finite-length dipole model, if t is held constant as it is here. The field near the electrode in the inner-layer region of the electrolyte double layer reaches very high values[26] but probably does not reach or exceed 10^8 V/cm at most. If the case (b) $\mu = 10.17$ D curve in fact applied to a monolayer of water in the inner layer region, there would be no dielectric saturation of this layer, even at the largest experimentally practical applied p.d. Even the case (b) $\mu = 1.85$ D curve would show little or no saturation under maximum voltage conditions. The $\mu = 17$ D Langevin curve would lead to great saturation, but the μ value used here was derived from relatively low field, very small saturation results on bulk water. Although a model which fits Grahame's[35] NaF double layer capacitance data quite well[26] strongly involves inner-layer Langevin-type dielectric saturation effects, there seem to be no independent data available concerning such effects for the inner layer or other molecular monolayers, and therefore the no-saturation prediction of the finite-length dipole model should not be dismissed out of hand.

Let us turn now to a consideration of unnormalized results for water at 20 °C. Curves for cases (a) and (b) and Langevin response are presented in Fig. 5 with $E(-1)$ as the abscissa. Note that

$$\sigma_M = \sigma(-1) = 8.85 \times 10^{-8} \times \epsilon_\infty E(-1) \mu\text{C/cm}^2$$

when E is expressed in V/cm, so the abscissa scale is proportional to σ_M. Here, we have again used $\mu = 17$ D for the Langevin curve and have adjusted $(\epsilon_{\text{eff}})_0$ to agree with that for the case (b) curve. This curve has the same parameters as that with $\omega_0 = 2.43$ in Fig. 4 and involves a value of T_N of 13.84. The case (a) curve, on the other hand, involves T_N of 33.89 and thus leads to $\omega_0 = 5.95$ for $\mu = 1.85$ D and $\eta = 0.124$. The results of Fig. 5 clearly show the very large differences between case (a) and (b) predictions for situations with the same d and μ. They also illustrate how much more readily saturation occurs for Langevin response than for the case (b) finite-length dipoles. On the other hand, the corresponding case (a) curve shows little or no change of ϵ_{eff} from $(\epsilon_{\text{eff}})_0$ within the entire likely experimental range of $E(-1)$. Note that $E(-1) = 10^8$ V/cm corresponds for this case to $\sigma_M = 8.85\,\mu\text{C/cm}^2$.

The maximum charge density at a given end of the finite-length dipoles when they are all lined up parallel, as would be the case at very low temperature with a small orienting field or at room temperature for an infinite orienting field, is $\sigma_{DM} = \eta e/d^2$, equal to about 20.6 μC/cm^2 for the present situation. On the $E(-1)$ scale, this charge density corresponds to about 3.9×10^7 V/cm for case (b) and 2.3×10^8 V/cm for case (a). At these fields the corresponding

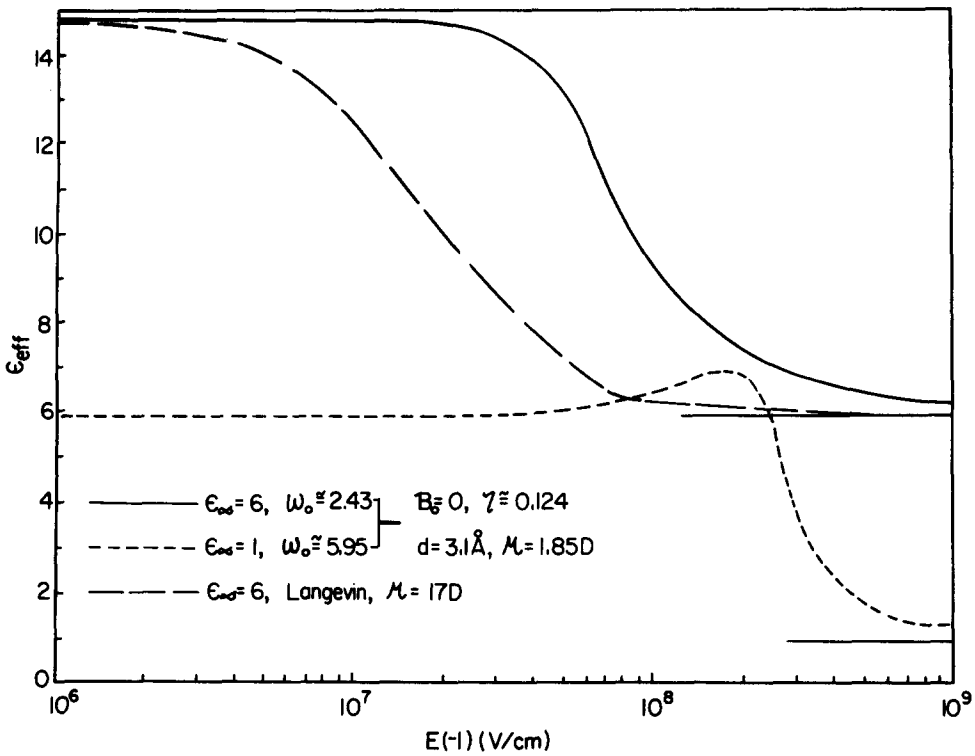

FIG. 5. Dependence of ϵ_{eff} on $E(-1)$ for Langevin case (b) and case (a) water-like situations.

curves show only a relatively small amount of saturation.

We complete our consideration of ϵ_{eff} behavior with the Table I summary of $(\epsilon_{eff})_0$ values for various situations. The initial choice, from which the other values follow, is in boldface. Some of the row 1–6 water results have already been mentioned. Here we have also presented values of C_{ILO}, the capacitance per unit area of the monolayer of thickness d and dielectric constant $(\epsilon_{eff})_0$. For the inner layer in aqueous NaF, it is about[22,26,35,36] 31 μF/cm^2. As shown in rows 3 and 4, this choice leads to a reasonable case (a) value for μ but an unlikely one for case (b), but it should be mentioned that the case (b) line 2 situation with $\mu = 1.85$ D may readily be made to yield a value of C_{ILO} of 31 μF/cm^2 if an additional thin region of field penetration into the metal electrode is included as well. This nonlocal electron overlap effect[22,36] can effectively lead to the presence of a very thin layer of low dielectric constant in series with the ordinary finite-length dipole molecular inner layer.

TABLE I. Values of $(\epsilon_{eff})_0$ for various conditions. Rows 1–6: H_2O at 20 °C; rows 7–10: CH_3Cl at − 20 °C. Odd rows: case (a); even rows: case (b).

	μ (Debyes)	$(\epsilon_{eff})_0$	C_{ILO} (μF/cm^2)
1	1.85	5.95	17.0
2		14.59	41.7
3	3.37	10.85	31.0
4	1.38		
5	24.89	80.1	229
6	10.16		
7	1.86	3.66	7.2
8		4.90	9.6
9	6.40	12.6	24.6
10	4.78		

Although the line 3 case (a) result is reasonable for the inner layer if one assumes that correlation effects have led to an augmented μ, it is the case (b) result which is much more appropriate for bulk water (rows 5 and 6). The case (a) situation even requires a η greater than unity. Of course, the present monolayer treatment should apply better to the inner layer than to bulk water in any event. It is interesting to note, however, that Morriss and Perram,[11] in a bulk water treatment using a tetrahedral arrangement of four charges to represent the multipole behavior of the water molecule, obtained, on taking some correlation into account, a value of $(\epsilon_{eff})_0$ of 13, far less than 80 and near our line-2 result.

In rows 7–10 we present results for CH_3Cl. Morriss and Cummings[12] applied their finite-length dipole theory for bulk dielectric constant behavior to this material and argued that its molecules involve nearly perfect finite-length electric dipoles. They obtained a − 20 °C value of $(\epsilon_{eff})_0$ of 10.3, 20% less than the experimental value of 12.6. Our case (a) results are with $\epsilon_\infty = 1$ and our case (b) ones use $\epsilon_\infty = n^2 = 1.79$, where n is the index of refraction. All results employ $d = N_V^{-1/3} = 4.53$ Å. Unfortunately, our row 9 and 10 values of μ, necessary to obtain $(\epsilon_{eff})_0 = 12.6$, are more augmented over the vapor-phase value of 1.87 D than seems likely. Again it appears that the present monolayer theory must be extended beyond its range of applicability to yield adequate bulk results.

Before leaving $(\epsilon_{eff})_0$ results, it is worth mentioning and illustrating a remarkably effective expression for bulk $(\epsilon_{eff})_0$ for polar, polarizable liquids which came out of our present finite-length dipole work. During our initial analysis of the present case (b) finite-length dipole problem with $B_0 = 0$, we inadvertently set to unity the denominator $\sinh(\omega_0)/\omega_0$ term from m_0 [see Eq. (A53)] and obtained $(\epsilon_{eff})_0/\epsilon_\infty = \cosh(\omega_0)$

instead of $(\epsilon_{\rm eff})_0/\epsilon_\infty = \omega_0 \coth(\omega_0)$. Note that ω_0^2 may be expressed as $4\pi N_V \mu^2/\epsilon_\infty kT$. Although the cosh result thus had no good theoretical justification (it follows when the finite-length dipole charge effects are properly accounted for but the part of the p.d. associated with the permanent dipoles is calculated as though their dipole moments were taken zero!), it has been found to have remarkable predictive value for a variety of materials and temperatures.[37] In its simplest form, involving no disposable parameters, one sets $\mu = \mu_V$, the vapor phase value of μ, and $\epsilon_\infty = n^2$. All correlation and reaction field effects are then accounted for by the form of the cosh function. Then ω_0^2 becomes just

$$4\pi N_V \mu_V{}^2/n^2 kT.$$

For water at 20 °C, the cosh formula yields $(\epsilon_{\rm eff})_0 \cong 77.2$ instead of 80.1, and for CH_3Cl at -20 °C it produces 13.9 instead of 12.6. Alternatively, one could again take $\epsilon_\infty = n^2$ and find that μ which yields perfect prediction of the experimental ϵ_B value. For water, the result is $\mu = 1.865$ D, only slightly larger than the 1.84 to 1.85 D value for μ_V. The predictive value of the cosh formula without disposable constants[37] is frequently superior to that of the much more complicated conventional Onsager–Kirkwood–Frohlich formula,[38] and it makes up for its current lack of adequate theoretical justification by its accuracy and simplicity.

We now return to the illustrative input value $\eta = 1/\sqrt{2}$ and show in Figs. 6 and 7 the field dependence of several quantities of interest for small and large ω_0. Figure 6 shows that $E^*(0) \equiv E_0^*$ is nearly a linear function of $E^*(-1)$ but $Q_D(1)$, the normalized dipole planar charge density at $y = 1$, reaches saturation near $E^*(1) = 4$, a region where dielectric saturation has begun but is still not extensive, as shown by the $\omega_0 = 1$, $B_0 = 0$ curve of Fig. 3. It is clear that as $Q_D(1)$ approaches saturation, $-\phi_D(1) = \phi_D(-1)$ reaches a maximum and then decreases. This dipole potential represents the integrated effect of the dipole field throughout its extent.

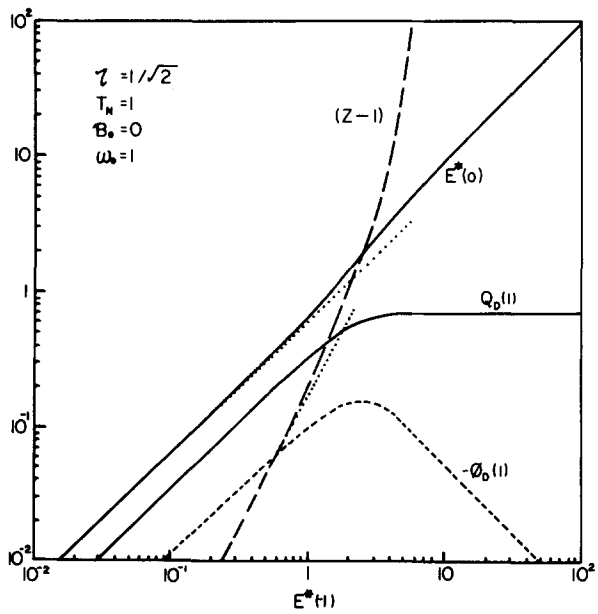

FIG. 6. Dependence of various normalized quantities on the normalized applied field for $\omega_0 = 1$.

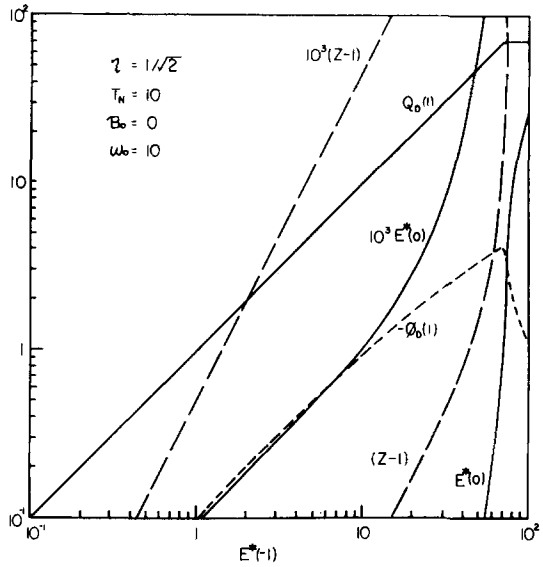

FIG. 7. Dependence of various normalized quantities on the normalized applied field for $\omega_0 = 10$.

As the field increases, the shielding also increases, so that the high field is confined to a small region. Thus the product of field and distance reaches a maximum and then begins to decrease. In this same region, Z begins to increase rapidly. Figure 7 shows somewhat similar behavior for $\omega_0 = 10$, but first $E^*(0)$ becomes nonlinear as expected in the region where $-\phi_D(1)$ reaches and exceeds unity and where $Q_D(1)$ and $-\phi_D(1)$ reach saturation and a maximum, respectively, at the much higher value $E^*(-1) \cong 70$. The linear growth of $Q_D(1)$ all the way to saturation is remarkable. The saturation value of $Q_D(1)$ is, as shown in the Appendix,

$$Q_{DM} = \eta T_N^2 = \omega_0^2/2\eta.$$

This result of course agrees with $\sigma_{DM}/\sigma_N = Q_{DM}$ when the previous expressions for σ_{DM} and σ_N are used. Now in the low field region, $(Z-1)$ is clearly proportional to $[E^*(-1)]^2$. Again the transition value $E^*(-1) = 70$ is near the point where the $\omega_0 = 10$ curve of Fig. 3 has just begun to show some dielectric saturation.

Figure 8 shows $Q_M = E^*(\pm 1)$ vs ϕ_a curves for several ω_0 values. For $\omega_0 = 1$, the effect of the permanent dipoles is almost negligible. However, for all the curves, there is a linear region for $0 \leqslant \phi_a \lesssim 1$, then a buildup as $Q_D(1)$ approaches its maximum value and then a final linear increase. Thus, the $\phi_a = 0$ intercept of the Q_M curve is just Q_{DM}. Now it may readily be shown from the case 2 equations in the Appendix that as $E_0^* \to \infty$,

$$Q_M = E_0^* + Q_D(1) \to E_0^* + Q_{DM},$$

and $\phi_a \to 2E_0^*$. Thus,

$$C_{SN} = Q_M/\phi_a \to 0.5 + (Q_{DM}/2E_0^*) \to 0.5.$$

Therefore,

$$\epsilon_{\rm eff} = 2\epsilon_\infty C_{SN} \to \epsilon_\infty,$$

as it should. These results show that the expression for the

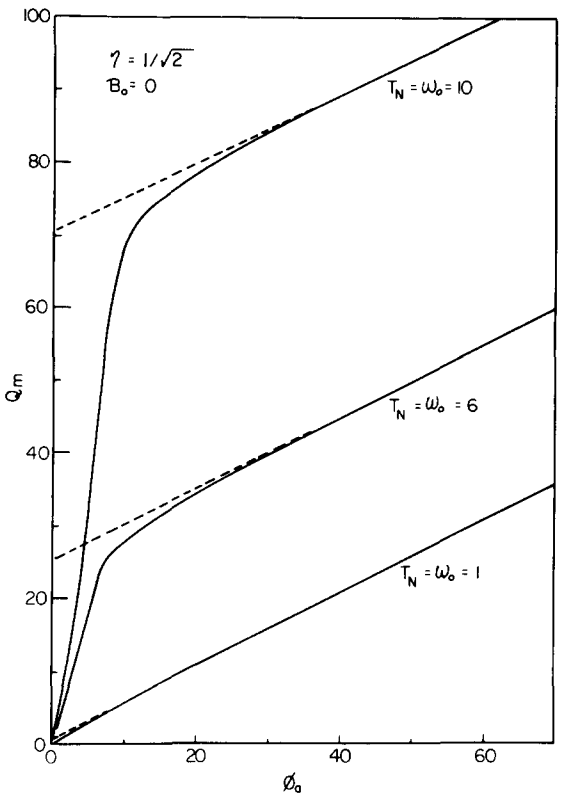

FIG. 8. Dependence of normalized electrode charge Q_m on normalized applied p.d. ϕ_a for several ω_0 values.

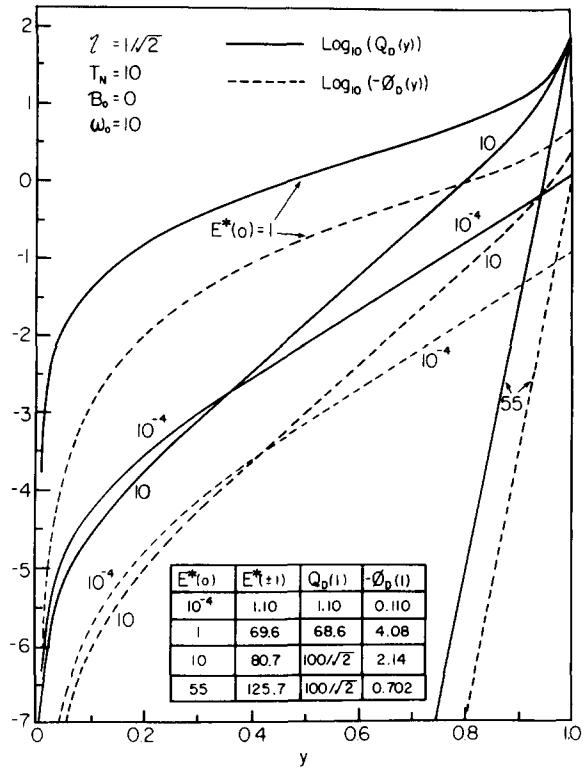

FIG. 9. Semilog plot of $Q_D(y)$ and $-\phi_D(y)$ on position y for various $E^*(0)$ values.

lines asymptotic to the final Q_M vs ϕ_a lines in Fig. 8 is

$$Q_M = 0.5\phi_a + (\omega_0^2/2\eta).$$

Finally, Fig. 9 shows a semilog plot of $Q_D(y)$ and $-\phi_D(y)$ vs y for $0 \leqslant y \leqslant 1$, several values of $E^*(0)$, and the relatively large value $\omega_0 = 10$. It is interesting that the $E^*(0) = 1$ curves lie higher over most of the range than those with $E^*(0)$ either smaller or larger. As $E^*(0)$ becomes larger than unity, we see that the distributed dipolar charge and the majority of the dipole contribution to the total p.d. become more and more concentrated near $|y| = 1$. For $E^*(0) = 55$, for example, $Q_D(y)$ and $-\phi_D(y)$ decrease nearly 4 orders of magnitude between $y = 1$ and $y = 0.9$. Thus as $E^*(1)$ and $E^*(0)$ increase, the present finite-length dipole model approaches closer and closer to the three-layer model discussed earlier. In this model the dipole charges are taken as $\delta(\pm 1)$ functions, thus all concentrated at $y = \pm 1$ and with their magnitude dependent on $E^*(0)$. But such concentration can occur in the present model only as $E^*(0) \to \infty$. There are thus fundamental differences between the models and these show up in many ways, especially in their different dielectric saturation predictions. Although the present model, which is here specialized for a molecular monolayer, is evidently not entirely applicable to a bulk liquid or even a dipolar single crystal with only a few allowed dipole orientations, its predictions and comparisons with those of other corresponding models are nevertheless instructive and useful. In a further paper dealing with the complete multilayer situation, results for $(\epsilon_{\text{eff}})_0$ in the limit of $\delta \to 0$ will be available for direct comparison with those from experiment and from other models for the bulk dielectric constant of a liquid.

ACKNOWLEDGMENTS

We appreciate the helpful suggestions of Professor Wayne Bowers and are grateful to the U. S. Army Research Office for support.

APPENDIX

In this Appendix, we solve the equations which lead to final expressions for the permanent-dipole-related quantities $Q_D(y)$ and $\phi_D(y)$ needed in Eqs. (26) and (27). In addition, we shall obtain a simplified closed-form expression for Z_T and expressions for ϵ_{eff} and $(\epsilon_{\text{eff}})_0$. The equations we need to solve and simplify are

$$Q_D(y) \equiv E_0^* Y(y) = -H \int_0^y \sinh[U_D(y')]\,dy', \tag{A1}$$

$$\phi_D(y) \equiv -E_0^* \int_0^y Y(y')\,dy', \tag{A2}$$

$$U_D(y) \equiv \eta[\phi(y) - \phi(-y)]$$
$$= -F\left[y - B\,\mathrm{sgn}(y) + \int_0^y Y(y')\,dy'\right], \tag{A3}$$

and

$$Z_T = 2\delta\cosh(\phi_0) + (1 - 2\delta)\Pi_\alpha Z, \tag{A4}$$

where

$$Z \equiv \int_0^1 \cosh[U_D(y)]\,dy, \tag{A5}$$

and $H \equiv H_0\Pi_\alpha/Z_T$,

$H_0 \equiv (1 - 2\delta)\eta T_N^2$,

$F \equiv 2\eta E_0^*$, $B \equiv B_0\Pi_\alpha/Z_T$, and

$B_0 \equiv 4\pi N_V(1 - 2\delta)(\alpha\beta)/\epsilon_\infty$.

The closed-form solution of the above coupled set of integral equations for $Y(y)$ turns out to be complicated but possible. From Eq. (A1), we may immediately derive

$$P(y)\equiv \frac{dY(y)}{dy} = -J\sinh[U_D(y)]. \tag{A6}$$

Let

$$P(0+)\equiv P_0 = -J\sinh(z_\alpha), \tag{A7}$$

where $J\equiv H/E_0^*$, $z_\alpha\equiv FB$, and we have used Eqs. (A6) and (A3) with $y=0+$. Next, Eq. (A3) leads to

$$\frac{dU_D(y)}{dy} = -F[1+Y(y)-2B\delta(y)]. \tag{A8}$$

Now on solving Eq. (A6) for $U_D(y)$ and differentiating, we find

$$\frac{dU_D(y)}{dy} = -\left(\frac{dP}{dy}\right)/(P^2+J^2)^{1/2}. \tag{A9}$$

Define $W(y)\equiv 1+Y(y)$ and write

$$dP/dy = (dW/dy)(dP/dW) = P(dP/dW).$$

Then on setting Eqs. (A8) and (A9) equal, we obtain

$$P(dP/dW)/(P^2+J^2)^{1/2} = F[W(y)-2B\delta(y)]. \tag{A10}$$

Now we shall collect terms and integrate from $y=0+$ to 1, noting that $Y(0+)=0$, $W(0+)=1$, and $P(0+)\equiv P_0\leqslant 0$. Then

$$F\int_1^W W'\,dW' = \int_{P_0}^P P'(P'^2+J^2)^{-1/2}\,dP'. \tag{A11}$$

This leads to

$$P^2 = P_0^2 + F(P_0^2+J^2)^{1/2}(W^2-1) + [(F/2)(W^2-1)]^2. \tag{A12}$$

Let $V\equiv W^2-1$ and note that

$$\left(\frac{dV}{dy}\right)^2 = (2P\sqrt{1+V})^2. \tag{A13}$$

Combining Eqs. (A12) and (A13) leads us to

$$\frac{dV}{dy} = \pm 2\sqrt{1+V}\,[P_0^2+F(P_0^2+J^2)^{1/2}V + (F/2)^2V^2]^{1/2}. \tag{A14}$$

This equation may be rewritten in the forms

$$\frac{dV}{dy} = \pm F[(1+V)(V_1+V)(V_2+V)]^{1/2} \equiv \pm F[(V-a)(V-b)(V-c)]^{1/2}, \tag{A15}$$

where we require $V\geqslant a>b>c$, and a, b, and c are always $\leqslant 0$. Specific choices of a, b, and c will be made below. It turns out that V_1 and V_2 may be expressed as

$$V_1 = (4J/F)\sinh^2(z_\alpha/2), \tag{A16}$$

$$V_2 = (4J/F)\cosh^2(z_\alpha/2), \tag{A17}$$

and thus

$$V_2 - V_1 = (4J/F), \tag{A18}$$

and

$$V_1V_2 = [(2J/F)\sinh(z_\alpha)]^2 = (2P_0/F)^2. \tag{A19}$$

Let us digress for a moment and consider some $E_0^*\to 0$ low-field limits of several quantities of interest. In this limit $\Pi_\alpha\to 1$, $Z\to 1$,

$$Z_T\to 2\delta+(1-2\delta)=1,$$

$$H\to H_0,\ F\to 0,\ B\to B_0,\ z_\alpha\to 0,\ JF\to 2\eta H_0,$$

$$V_2\to\infty,\ P_0\to 2\eta H_0B_0,$$

and

$$V_1\to V_{10}\equiv 2\eta H_0B_0^2.$$

The last form of Eq. (A15) is necessary for integration in terms of an incomplete elliptic integral. But because of the wide variation of V_1 and V_2 with E_0^*, a single identification of (a,b,c) and $(1,V_1,V_2)$ is insufficient. Table II shows the three cases of possible interest. Case 1 applies for sufficiently small B and E_0^* that $V_1<1$ and $V_2\geqslant 1$. As E_0^* increases from zero, cases 1 and 2 coalesce at the E_0^* which leads to $V_2=1$. This E_0^*, E_{01}^*, may be calculated using Eq. (A17) in general, but when $\alpha=0$ so $B=0$, it is given by the implicit relation $E_{01}^* = \pm\sqrt{2H/\eta}$. Since we shall always take $E^*(-1)\geqslant 0$, we may take the plus sign here. For $E_0^*\geqslant E_{01}^*$, case 2 is applicable. Case 3 need be considered only when $V_{10}\geqslant 1$, a possibility for sufficiently large B_0. Note that when $\delta=0$, e.g., $B=B_0/Z$. Because of the rapid growth of Z as E_0^* increases, B and z_α will decrease as E_0^* increases from zero. Thus, for $\delta=0$ case, the $V_1\geqslant 1$ situation is most likely to occur at $E_0^*\to 0$. For the $\delta=0$, $\alpha\neq 0$ calculations in the present paper, we shall always deal with sufficiently small α and B_0 values that $V_{10}<1$ and thus case 3 need not be considered further.

Let us define

$$I(a,V)\equiv\int_a^V \frac{dV'}{[(V'-a)(V'-b)(V'-c)]^{1/2}}. \tag{A20}$$

Then using Eqs. (A15) and (A20), we may write

$$\pm F\int_{0+}^y dy' = \pm Fy = I(0,V)\equiv I(a,0)+I(a,V). \tag{A21}$$

We shall need result No. 237.00 of Ref. 39,

$$I(a,V) = g_0\,sn^{-1}[\sqrt{V-a}/\sqrt{V-b},\,k], \tag{A22}$$

where

$$g_0\equiv 2/(a-c)^{1/2},$$

$$k^2\equiv(b-c)/(a-c), \tag{A23}$$

and

$$k'^2\equiv 1-k^2=(a-b)/(a-c). \tag{A24}$$

Here sn is a Jacobian elliptic function. Reference 39 is a very useful comprehensive compendium of elliptic integral and elliptic function relations. Let us further define

$$\omega\equiv F/g_0 = (F/2)\sqrt{a-c} = \sqrt{JF}\,[(F/4J)(a-c)]^{1/2}. \tag{A25}$$

TABLE II. Possible choices for (a, b, c) for elliptic integral integration.

Case	$-a$	$-b$	$-c$
1	V_1	1	V_2
2	V_1	V_2	1
3	1	V_1	V_2

We assume, as discussed above, that as $E_0^* \to 0$, case 1 rather than case 3 applies. Then in this limit

$$\omega \to \sqrt{JF} \to (2\eta H_0)^{1/2} \equiv \omega_0, \tag{A26}$$

and $P_0 \to \omega_0^2 B_0$,

$$V_1 \to V_{10} = (\omega_0 B_0)^2.$$

Equations (A21) and (A22) now yield

$$\pm \omega y \equiv u = sn^{-1}[\sqrt{a/b}, k] + sn^{-1}[\sqrt{V-a}/\sqrt{V-b}, k]. \tag{A27}$$

Since $Y(y)$ is, from physical considerations, even in y and thus $V(y)$ is also even, we must replace $\pm y$ in Eq. (A27) by $|y|$, but since we need be concerned only with $0 \leqslant y \leqslant 1$, we shall omit this refinement. Next define

$$a_0 \equiv sn^{-1}[\sqrt{a/b}, k], \tag{A28}$$

and

$$u_a \equiv u - a_0. \tag{A29}$$

We may solve Eq. (A27) for V, obtaining

$$V = [a - bsn^2(u_a)]/[1 - sn^2(u_a)] = nc^2(u_a)[a - bsn^2(u_a)], \tag{A30}$$

where we have omitted the k-modulus argument of the elliptic functions for simplicity and introduced the additional elliptic function

$$nc(u_a) \equiv [cn(u_a)]^{-1}.$$

Finally, on transforming back to $Y(u_a)$, we find

$$Y(u_a) = nc(u_a)[(a+1) - (b+1)sn^2(u_a)]^{1/2} - 1, \tag{A31}$$

where we have selected the plus sign of the $\pm$ on physical grounds. Equation (A31) is our general solution of the original equations. Note that it leads to $Y(u_a) = 0$ at $u = 0$ and $\pm 2a_0$.

We may now use Eqs. (A6) and (A31) to obtain

$$P(u_a) = \frac{\omega(a-b)tn(u_a)dc(u_a)}{[(a+1) - (b+1)sn^2(u_a)]^{1/2}}, \tag{A32}$$

which leads to an explicit expression for $U_D(u_a)$ through Eq. (A6),

$$U_D(u_a) = -\sinh^{-1}[P(u_a)/J]. \tag{A33}$$

When this result is combined with Eqs. (A2) and (A3), we can obtain an expression for $\phi_D(y)$ indirectly since the direct integration of Eq. (A31) in the general case seems very difficult. We obtain

$$-\phi_D(y)/E_0^* \equiv I_Y = \int_{0+}^{y} Y(y')dy' = B\,\mathrm{sgn}(y) - y + F^{-1}\sinh^{-1} \times \left[\frac{\omega(a-b)tn(u_a)dc(u_a)}{J[(a+1) - (b+1)sn^2(u_a)]^{1/2}}\right], \tag{A34}$$

remembering that $u_a \equiv \omega y - a_0$. In the above, $tn \equiv sn/cn$ and $dc \equiv dn/cn$, where dn is another Jacobian elliptic function.

Let us now obtain a general expression for Z using the foregoing results. First, from Eqs. (A6) and (A7) we obtain

$$\sqrt{1 + (P_0/J)^2} = \cosh(z_\alpha) \tag{A35}$$

and

$$\sqrt{1 + (P/J)^2} = \cosh[U_D(y)]. \tag{A36}$$

Now Eq. (A12) may be rewritten as

$$(F/2J)(W^2 - 1) = \sqrt{1 + (P/J)^2} - \sqrt{1 + (P_0/J)^2} = \cosh[U_D(y)] - \cosh(z_\alpha). \tag{A37}$$

Since $W^2 - 1 \equiv V$, we may use Eq. (A30) to write

$$\cosh[U_D(y)] = \cosh(z_\alpha) + (F/2J)[a \cdot nc^2(u_a) - b \cdot tn^2(u_a)]. \tag{A38}$$

Now Eq. (A5) may be rewritten as

$$Z = \omega^{-1}\int_{-a_0}^{\omega - a_0} \cosh[U_D(u_a)]du_a = \cosh(z_\alpha) + (F/2J)\left[a + \frac{(a-b)}{\omega k'^2}[dn(u_{al})tn(u_{al}) + dn(a_0)tn(a_0) - E(u_{al}) - E(a_0)]\right], \tag{A39}$$

where we have set

$$u_{al} \equiv (u_{al})_{y=1} = \omega - a_0$$

and have used integrals listed in Ref. 39. Here $E(u_{al})$ is the incomplete elliptic integral of the second kind; it also involves the modulus k. If, as usual, we restrict attention to cases 1 and 2 only, a $= -V_1$ and

$$\cosh(z_\alpha) + (Fa/2J) = \cosh(z_\alpha) - 2\sinh^2(z_\alpha/2) \equiv 1. \tag{A40}$$

Now since

$$(F/2J)(a-b)/(\omega k'^2) = 2\omega/JF,$$

we obtain for cases 1 and 2 the general result

$$Z = 1 + (2\omega/JF)\{dn(u_{al})tn(u_{al}) + dn(a_0)tn(a_0) - E(u_{al}) - E(a_0)\}. \tag{A41}$$

Since tn and E are odd functions of their principal arguments, it is obvious that $Z \to 1$ as $w \to 0$. In fact, it can be shown from Eq. (A41) that as $E_0^* \to 0$, a limit which yields $k'^2 \to 1$, then $Z \to 1$ for any consistent ω_0 and a_{00} values, where a_{00} is the limit of a_0 as $E_0^* \to 0$. Although Eq. (A41) holds for both case 1 and 2, the expressions for a_0 and ω are different for the two cases.

Now we shall specialize our other general results for cases 1 and 2, remembering that case 1 is appropriate as $E_0^* \to 0$ and 2 as $E_0^* \to \infty$. Table III gives expressions for some of the quantities of interest in these cases. At the transition field between these two cases, $V_2 = 1$, $k' = 1$, $V_1 = 1 - (4J/F)$, and all corresponding case-1 and case-2 quantities are equal. For case 1, Eq. (A31) yields

$$Y(u_a) = cn(a_0)nc(u_a) - 1, \tag{A42}$$

TABLE III. Comparison of various quantities for cases 1 and 2.

Quantity	Case 1	Case 2
a_0	$sn^{-1}(\sqrt{V_1})$	$sn^{-1}\{\tanh(z_\alpha/2)\}$
$cn(a_0)$	$\sqrt{1 - V_1}$	$\mathrm{sech}(z_\alpha/2)$
$cd(a_0)$	$\mathrm{sech}(z_\alpha/2)$	$\sqrt{1 - V_1}$
k'^2	$(F/4J)(1 - V_1)$	$[(F/4J)(1 - V_1)]^{-1}$
ω	$\sqrt{JF}$	$(F/2)\sqrt{1 - V_1}$

which clearly leads to $Y(u_a)=0$ at $y=0$. Now we can obtain expressions for I_Y and thus $\phi_D(y)$ both from Eq. (A34) and by direct integration[39]; the results are, respectively,

$$I_Y = B\,\mathrm{sgn}(y) - y + F^{-1}\sinh^{-1}[2k'tn(u_a)dc(u_a)] \tag{A43}$$

and

$$I_Y = -y + 2F^{-1}\ln\left[\frac{k'tn(u_a)+dc(u_a)}{-k'tn(a_0)+dc(a_0)}\right], \tag{A44}$$

where we have used

$$\omega(a-b)/J\sqrt{1-V_1} = 2k'$$

in obtaining Eq. (A43). On setting Eq. (A43) equal to Eq. (A44), one obtains an interesting, complicated and apparently novel relation between elliptic functions. It can be further simplified through the identities.

$$FB/2 \equiv z_\alpha/2 \equiv \cosh^{-1}[dc(a_0)] \equiv -\ln[dc(a_0)-k'tn(a_0)]. \tag{A45}$$

Next we require an expression for the total p.d. across the layer:

$$\phi_a \equiv \Delta\phi = \phi(-1)-\phi(1) = -\eta^{-1}U_{D1},$$

where $U_{D1}\equiv U_D(y)$ at $y=1$. From Eqs. (A3) and (A34), we may immediately write

$$\phi_a = \eta^{-1}F[1-B+I_{Y1}], \tag{A46}$$

where I_{Y1} is the value of I_Y at $y=1$, where $u_a=u_{al}$. The two expressions for I_Y above lead to two equivalent expressions for ϕ_a. They may be simplified to yield the case-1 results,

$$\begin{aligned}\phi_a &= 2\eta^{-1}\ln[dc(u_{al})+k'tn(u_{al})]\\ &= 2\eta^{-1}\cosh^{-1}[dc(u_{al})]\\ &= \eta^{-1}\sinh^{-1}[2k'tn(u_{al})dc(u_{al})].\end{aligned} \tag{A47}$$

Since $k'\to 0$ as $E_0^*\to 0$,

$$\phi_a \to 2E_0^*\omega_0^{-1}\sqrt{1-V_{10}}\sinh(\omega_0-a_{00})$$

also approaches zero in this limit as it should.

In case 2, Eq. (A31) leads, after some manipulation, to

$$Y(u_a) = cd(a_0)dc(u_a) - 1, \tag{A48}$$

which again yields $Y(u_a)=0$ at $y=0$. Note that $dn(a_0)=\sqrt{c/b}$ in general and is therefore unity at the transition field. Further, since $k^2\to 0$ at this field, $dn(u_a)$ is also unity at that point[39] and expressions (A42) and (A48) are identical as they must be. We can again obtain two different but equivalent expressions for I_Y in the present case but shall not list them. To obtain ϕ_a we may use U_{D1} with Eqs. (A32) and (A33) to yield

$$\phi_a = \eta^{-1}\sinh^{-1}\left[\frac{2cd(a_0)tn(u_{al})dc(u_{al})}{[(1-V_1)-(1-V_2)sn^2(u_{al})]^{1/2}}\right], \tag{A49}$$

where we have used

$$\omega(a-b)/J = 2\sqrt{1-V_1} = 2cd(a_0)$$

for the present case. It is clear that this expression and those in Eq. (A47) yield the same result at the transition point where V_2, k', and dn are all unity.

Next let us take $\delta=0$ and consider the case $2E_0^*\to\infty$ limiting forms of Q_{D1}, the $y=1$ value of $Q_D(y)$, and Z. Now as E_0^* increases, $k'^2\to 0$, and V_1, V_2 J, H, and a_0 all approach zero as well. We first consider the limiting form of Eq. (A41). Then $(2\omega/JF)\to J^{-1}$,

$$\begin{aligned}&E(u_{al},k)\to E(u_{al},1)=\tanh(u_{al}),\\ &(dntn-E)\to(dnsn-cn\cdot E)/cn\\ &\to(dn\cdot\tanh-cn\cdot\tanh)/cn=\tanh\cdot[(dn-cn)/cn].\end{aligned}$$

Now we may employ the $k'^2\to 0$ approximation formulas 127.02 of Ref. 39 to express $(dn-cn)/cn$ as $0.5k'^2\sinh^2$ in the $k'^2\to 0$ limit. Since $a_0\to 0$,

$$u_{al}\to\omega\to F/2=\eta E_0^*.$$

Therefore, $\tanh(u_{al})\to 1$ and $\tanh(a_0)\to 0$. Finally, we obtain from Eq. (A41),

$$\begin{aligned}Z &\to 1+(k'^2/2J)\sinh^2(\omega)\\ &\to(2/F)\sinh^2(\omega)\to(\eta E_0^*)^{-1}\sinh^2(\eta E_0^*)\to\infty,\end{aligned} \tag{A50}$$

showing how Z approaches infinity for large E_0^*. Next, let us evaluate Eqs. (A1) and (A42) at $y=1$ for $E_0^*\to\infty$. On using the results above, we may write

$$\begin{aligned}Q_{D1} &\to 0.5E_0^*k'^2\sinh^2(\omega)\\ &\to 0.5E_0^*(4J/F)\sinh^2(\omega)\\ &\to(2/F)(H_0/Z)\sinh^2(\omega)=H_0\eta T_n^2\equiv Q_{DM}.\end{aligned} \tag{A51}$$

Finally, let us derive an expression for ϵ_{eff} and $(\epsilon_{\mathrm{eff}})_0$ for the monolayer with $\delta=0$. The static capacitance per unit area C_S is given by $\epsilon_{\mathrm{eff}}/4\pi d$, by definition of ϵ_{eff}. Now since $C_N\equiv\epsilon_\infty/4\pi t$,

$$C_{SN}\equiv C_S/C_N=\epsilon_{\mathrm{eff}}/2\epsilon_\infty.$$

Therefore, $\epsilon_{\mathrm{eff}}=2\epsilon_\infty C_{SN}$. But C_{SN} is just $E^*(-1)/\phi_a$, and, from Eq. (20),

$$E^*(-1)=Q_{D1}+E_0^*$$

when $Q_I=0$. It follows that

$$E^*(-1)=E_0^*\{1+Y(1)\}=E_0^*W(1).$$

Since we are interested in the $E_0^*\to 0$ limit, we use case-1 results. We may determine $W(1)$ from Eq. (A42) and ϕ_a from Eq. (A47). Then

$$\epsilon_{\mathrm{eff}} = \frac{2\eta\epsilon_\infty E_0^*cn(a_0)nc(u_{al})}{\sinh^{-1}[2k'tn(u_{al})dc(u_{al})]}. \tag{A52}$$

A similar expression applying in the case-2 field region is readily derived. We now consider the $E_0^*\to 0$ limit of Eq. (A52) to obtain a result for $(\epsilon_{\mathrm{eff}})_0/\epsilon_\infty$. On using

$$cn(a_0)=\sqrt{1-V_1},$$

remembering that $k'^2\to 0$, and that in this limit

$$\begin{aligned}&nc(u_{al})\to\cosh(u_{al}),\\ &tn(u_{al})\to\sinh(u_{al}),\\ &dc(u_{al})\to 1,\ \omega\to\omega_0\equiv 2\eta H_0,\end{aligned}$$

and

$$k'\to\sqrt{F/4J}\sqrt{1-V_1}$$

with $J\to H_0/E_0^*$, we find

$$(\epsilon_{\rm eff})_0/\epsilon_\infty = \omega_0 \coth(\omega_0 - a_{00}), \tag{A53}$$

where

$$a_{00} \equiv sn^{-1}(\sqrt{V_{10}}) = sn^{-1}(\omega_0 B_0).$$

Finally, on using $\tanh(a_{00}) = \omega_0 B_0$, we may rewrite Eq. (A53) in the form

$$(\epsilon_{\rm eff})_0/\epsilon_\infty = \{\omega_0 \coth(\omega_0)\}\left[\frac{1-\omega_0 B_0 \tanh(\omega_0)}{1-\omega_0 B_0 \coth(\omega_0)}\right]. \tag{A54}$$

This expression has a pole at $B_0 = \omega_0^{-1}\tanh(\omega_0)$, but as long as this condition is not closely satisfied and $\tanh(\omega_0) \cong 1$, $(\epsilon_{\rm eff})_0/\epsilon_\infty$ is closely given by $\omega_0 \coth \omega_0 \cong \omega_0$, virtually independent of B_0. Finally, it should be mentioned that all the foregoing results also apply when $\alpha = 0$ so that B, B_0, z_α, a_0, and V_1 are all identically zero. Actual numerical calculations of the various elliptic functions needed in this work have been carried out using the very rapidly convergent arithmetic–geometric averaging method.[40]

[1] G. Gouy, J. Phys. Radium **9**, 457 (1910).
[2] D. L. Chapman, Philos. Mag. **25**, 475 (1913).
[3] L. Blum, J. Phys. Chem. **8**, 136 (1977).
[4] D. Henderson and L. Blum, J. Chem. Phys. **69**, 5441 (1978).
[5] S. Levine and C. W. Outhwaite, J. Chem. Soc. Faraday Trans. 2 **74**, 1960 (1978).
[6] D. Henderson, L. Blum, and W. R. Smith, Chem. Phys. Lett. **63**, 381 (1979).
[7] C. W. Outhwaite, L. B. Vuiyan, and S. Levine, J. Chem. Soc. Faraday Trans. 2 **76**, 1388 (1980).
[8] D. Henderson and L. Blum, Surf. Sci. **101**, 189 (1980).
[9] D. Henderson and L. Blum, Can. J. Chem. **59**, 1906 (1981).
[10] D. Henderson and L. Blum, J. Electroanal. Chem. **132**, 1 (1982).
[11] G. P. Morriss and J. W. Perram, Mol. Phys. **43**, 670 (1981).
[12] G. P. Morriss and P. T. Cummings, Mol. Phys. **45**, 1099 (1982).
[13] F. Vericat and L. Blum, J. Chem. Phys. **77**, 5808 (1982).
[14] G. P. Morriss and P. A. Monson, Mol. Phys. **48**, 181 (1983).
[15] J. R. Macdonald, D. R. Franceschetti, and A. P. Lehnen, J. Chem. Phys. **73**, 5272 (1980).
[16] J. R. Macdonald, J. Chem. Phys. **75**, 3155 (1981).
[17] A. P. Lehnen and J. R. Macdonald, Cryst. Lattice Defects **9**, 149 (1983).
[18] J. R. Macdonald, A. P. Lehnen, and D. R. Franceschetti, J. Phys. Chem. Solids **43**, 39 (1982).
[19] J. R. Macdonald, D. R. Franceschetti, and A. P. Lehnen, Solid State Ionics **5**, 105 (1981).
[20] S. H. Liu, Surf. Sci. **101**, 49 (1980).
[21] J. R. Macdonald, Surf. Sci. **116**, 135 (1982).
[22] J. R. Macdonald and S. H. Liu, Surf. Sci. **125**, 653 (1983).
[23] J. J. van der Klink, D. Rytz, F. Bursa, and U. Hochli, Phys. Rev. B **27**, 89 (1983).
[24] K. B. Oldham and R. Parsons, Electrokhimiya **13**, 866 (1977).
[25] P. Dalrymple-Alford and K. B. Oldham, Can. J. Chem. **56**, 861 (1978).
[26] J. R. Macdonald and C. A. Barlow, Jr., J. Chem. Phys. **36**, 3062 (1962).
[27] R. H. Fowler, *Statistical Mechanics*, 2nd ed. (Cambridge University, Cambridge, England, 1936), pp. 452–453.
[28] A. R. von Hippel, in *Dielectric Materials and Applications*, edited by A. R. von Hippel (Wiley, New York, 1954), pp. 39–40.
[29] L. Onsager, J. Am. Chem. Soc. **58**, 1486 (1936).
[30] J. G. Kirkwood, J. Chem. Phys. **7**, 911 (1939).
[31] J. R. Macdonald and C. A. Barlow, Jr., J. Chem. Phys. **39**, 412 (1963); **40**, 237 (1964).
[32] S. Levine, G. M. Bell, and A. L. Smith, J. Phys. Chem. **73**, 3534 (1969).
[33] W. R. Fawcett and R. M. de Nobriga, J. Phys. Chem. **86**, 371 (1982).
[34] H. A. Kolodziej and G. P. Jones, J. Chem. Soc. Faraday Trans. 2 **71**, 269 (1975).
[35] D. C. Grahame, J. Am. Chem. Soc. **76**, 4819 (1954).
[36] A. A. Kornyshev and M. A. Vorotyntsev, Surf. Sci. **101**, 23 (1980); Can. J. Chem. **59**, 1031 (1981). See, also, Electrochim. Acta **26**, 1 (1981).
[37] J. R. Macdonald and S. W. Kenkel, J. Phys. D **16**, L195 (1983).
[38] C. J. F. Bottcher, *Theory of Electric Polarisation* (Elsevier, Amsterdam, 1973), Vol. I.
[39] P. F. Byrd and M. D. Friedman, *Handbook of Elliptic Integrals for Engineers and Physicists* (Springer, Berlin, 1954).
[40] L. M. Milne-Thomson, in *Handbook of Mathematical Functions*, edited by M. Abramowitz and I. Stegun (Dover, New York, 1964), pp. 598 and 599.